Chemical Science

ROYAL SOCIETY OF CHEMISTRY

EDGE ARTICLE

View Article Online
View Journal | View Issue

Cite this: *Chem. Sci.*, 2020, **11**, 4817

All publication charges for this article have been paid for by the Royal Society of Chemistry

Dialumenes – aryl *vs.* silyl stabilisation for small molecule activation and catalysis†

Catherine Weetman, Amelie Porzelt, Prasenjit Bag, Franziska Hanusch and Shigeyoshi Inoue *

Received 16th March 2020
Accepted 17th April 2020

DOI: 10.1039/d0sc01561j

rsc.li/chemical-science

Main group multiple bonds have proven their ability to act as transition metal mimics in the last few decades. However, catalytic application of these species is still in its infancy. Herein we report the second neutral NHC-stabilised dialumene species by use of a supporting aryl ligand (**3**). Different to the *trans*-planar silyl-substituted dialumene (**3^{Si}**), compound **3** features a *trans*-bent and twisted geometry. The differences between the two dialumenes are explored computationally (using B3LYP-D3/6-311G(d)) as well as experimentally. A high influence of the ligand's steric demand on the structural motif is revealed, giving rise to enhanced reactivity of **3** enabled by a higher flexibility in addition to different polarisation of the aluminium centres. As such, facile activation of dihydrogen is now achievable. The influence of ligand choice is further implicated in two different catalytic reactions; not only is the aryl-stabilised dialumene more catalytically active but the resulting product distributions also differ, thus indicating the likelihood of alternate mechanisms simply through a change of supporting ligand.

Introduction

The ability to isolate and stabilise complexes containing metal–metal bonds is of fundamental interest, providing both experimental and theoretical insights into the intrinsic nature of the metal centre.[1] Since the discovery that the so-called 'double bond rule' could be broken in the beginning of the last quarter of the 20th century,[2–5] efforts within main group chemistry have strived towards isolating a plethora of both homo- and hetero-main group element multiply bonded compounds, which have been the subject of numerous reviews.[6,7] Aside from curiosity, one of the driving forces behind this research area is the ability to use main group multiple bonds as transition metal mimics.[8–10] This is possible due to similarly energetically accessible frontier molecular orbitals. Thus, reduction of small molecules, such as dihydrogen, under ambient conditions by sustainable main group metal centres is achievable.[11]

Whilst the ability to mimic transition metals is now possible in regard to oxidative addition reactions, main group elements still fall short in terms of catalytic activity due to the resulting stability of the higher oxidation state complexes, *i.e.* the first step in a redox based catalytic cycle. In order to truly compete with transition metals that are currently employed in industry, the ability to influence the stability, and thus reactivity, of main group metal centres is paramount. One method of influencing stability is through choice of stabilising ligand. If you consider disilenes, the choice of silyl, aryl and nitrogen-based ligands has been shown to influence the structural parameters around the double bond,[12,13] with silyl groups tending towards *trans*-planar geometries[13] and aryl groups promoting *trans*-bent character. It was not until the use of an N-heterocyclic imine (NHI) based ligand, which results in a highly *trans*-bent and twisted geometry, that dihydrogen activation was achieved.[14]

An electropositive silyl supporting ligand was used to stabilise the first neutral aluminium–aluminium double bond, namely dialumene.[15] DFT calculations found the HOMO to consist of a π-bond formed from almost pure Al p-orbitals and as such a planar geometry was observed. As predicted, the dialumene behaved as a transition metal mimic towards a variety of small molecules, as well as enabling catalytic reduction of CO_2.[16] Prior to the isolation of the first neutral dialumene, several compounds with Al–Al bond orders greater than 1 were isolated.[17] These can be classed as radical mono-anionic species, one electron π-bonded compounds, a dianionic complex and masked dialumenes. The stick with latter, reported independently by Power[18] and Tokitoh,[19] proposed the intermediacy of aryl-stabilised dialumenes, with the masked species being a result of [2 + 4]-cycloaddition reaction due to the use of aromatic solvent. This was additionally accounted for through a series of [2 + 2]-cycloaddition reactions with internal alkynes. Tokitoh further showed that the benzene derived masked species was capable of activating dihydrogen;[20] however, upon switching to an anthracene derived masked species no reactivity towards dihydrogen was observed.

Department of Chemistry, Catalysis Research Center and Institute of Silicon Chemistry, Technische Universität München, Lichtenbergstra ße 4, 85748, Garching bei München, Germany. E-mail: s.inoue@tum.de

† Electronic supplementary information (ESI) available. CCDC 1989167–1989172. For ESI and crystallographic data in CIF or other electronic format see DOI: 10.1039/d0sc01561j

On descending group 13, heavier digallenes and dithallenes have been isolated which show notable *trans*-bent character and have been known to dissociate to their corresponding monomers in hydrocarbon solutions.[21–25] However, digallanes have been shown to react as the double bonded species, rather than the monomer with regards to cycloadditions of unsaturated C–C bonds and even dihydrogen activation.[26–28]

Motivated by our group's previous efforts in dialumene chemistry, we targeted the isolation of a neutral aryl-stabilised dialumene to compare the intrinsic nature of the aluminium–aluminium double bond through the influence of ligand stabilisation. Whilst silyl and aryl groups have been routinely used in main group multiple bond chemistry, no direct comparisons of their influence on multiple bonds as reactive species have been drawn. As such, we proposed a systematic study of both dialumenes towards activation of a range of small molecules and their use in catalysis, with the aim of providing experimental and theoretical insight into the influence of these ligand classes on main group multiple bond reactivity.

Results and discussion

Synthesis of aryl-stabilised dialumene

Following on from the successful isolation of the first neutral dialumene, we focused our attention on expanding the scope of this class of compounds towards aryl stabilised systems. As such, we targeted the use of the Tipp ligand (Tipp = 2,4,6-tri-*iso*-propylphenyl) for the stabilisation of a new dialumene. In keeping with the previous dialumene, the choice of N-heterocyclic carbene (NHC) remained the same, I^{i}Pr$_2$Me$_2$ (I^{i}Pr$_2$Me$_2$ = 1,3-di-*iso*-propyl-4,5-dimethyl-imidazolin-2-ylidene). Direct reaction of I^{i}Pr$_2$Me$_2$AlH$_3$ and LiTipp at −78 °C resulted in formation of the monosubstituted aluminium dihydride complex I^{i}Pr$_2$Me$_2$Al(Tipp)H$_2$ (**1**) (Scheme 1) in good yield (66%, ^{27}Al: δ 112.9 ppm).[29] The identity of compound **1** was confirmed upon inspection of the ^{1}H NMR spectrum wherein three resonances for the *iso*-propyl groups were identified in a 2 : 2 : 1 ratio (NHC : *o*-Tipp : *p*-Tipp *iso*-propyl signals) as well as a characteristic broad signal for the Al–H$_2$ protons (^{1}H: δ 5.11 ppm). Additionally, a sharp IR stretching band at 1711 cm^{-1} (Al–H) was observed in the IR spectrum.

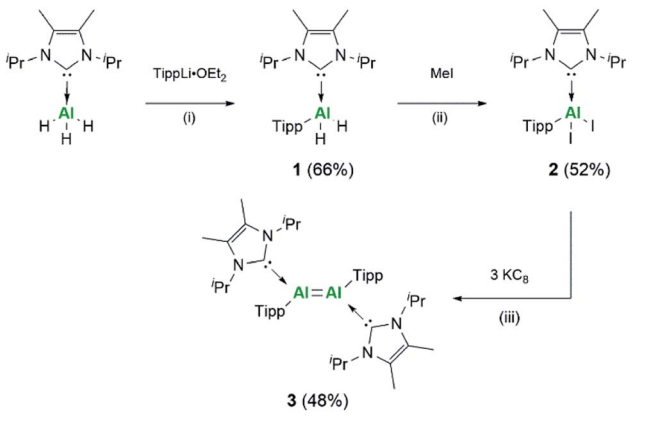

Scheme 1 Synthesis of aryl substituted Al compounds, Tipp = 2,4,6-tri-*iso*-propylphenyl. Reaction conditions: (i) TippLi·OEt$_2$, Et$_2$O −78 °C to RT 48 h; (ii) MeI, toluene 0 °C to RT 24 h; (iii) 3 eq. of KC$_8$, C$_6$H$_6$, RT 72 h.

Conversion of **1** towards formation of I^{i}Pr$_2$Me$_2$Al(Tipp)I$_2$ (**2**) could be achieved through reaction with BI$_3$·dms (dms = dimethyl sulfide) or with a small excess of methyl iodide, with the latter resulting in higher and cleaner conversion; moreover, the concomitant formation of methane allows for facile reaction monitoring. Loss of signals relating to Al–H were observed in both the ^{1}H NMR and IR spectra, and further characterisation by single crystal XRD confirmed the identity of **2** (Fig. S54†). Compound **2** is structurally analogous to the corresponding silyl supported complex (**2^{Si}**) with Al–C^{NHC} bond lengths essentially the same (**2**: 2.0645(18) Å; **2^{Si}**: 2.0673(17) Å), indicating the dative nature of the NHC ligand. This is additionally confirmed on comparison with the Al–C^{Tipp} bond length (1.9887(19) Å), which is smaller than the sum of the covalent radii (R_{Al-C} = 2.01 Å).[30]

Following the analogous synthetic protocol to the silyl dialumene, compound **2** was stirred vigorously with KC$_8$ at room temperature (Scheme 1). Through monitoring the reaction by ^{1}H NMR, it was found that this reaction requires 72 hours rather than the 24 hours required for the previous case. Compound **3** was isolated as a black solid, and in contrast to the silyl stabilised dialumene (**3^{Si}**), **3** is highly soluble in a broad range of aromatic, alkyl and ethereal solvents. Both dialumenes are stable in the solid state in an inert atmosphere for prolonged periods; however, they decompose in solution after 24 hours. The ^{1}H NMR spectrum of **3** shows a large broad signal at room temperature (~7.0–5.5 ppm) which resolves into distinct signals at 228 K for the *iso*-propyl groups, indicating a degree of rotational fluxionality in this system (Fig. S11†).

Single crystals were grown from a concentrated *n*-hexane solution at 5 °C and revealed a *trans*-bent and twisted geometry of the aryl stabilised dialumene (compound **3**, Fig. 1) (θ = 17.25°, 23.70°, τ = 12.06°), which contrasts with the *trans*-planar geometry observed previously. Furthermore, in **3^{Si}** the NHC groups were found to be parallel to each other, whilst in **3** they are found to be almost perpendicular (85°). The change from a planar to a *trans*-bent and twisted geometry has also been observed in disilene chemistry on switching between aryl and silyl-based ligands.[12,13] The Al–Al bond length is 2.4039(8) Å which is fractionally longer than that in the previous dialumene (**3^{Si}**: 2.3943(16) Å). Another notable difference between the two systems lies in the Al–C$_{NHC}$ bond length (**3**: 2.0596(16), 2.0422(17); **3^{Si}**: 2.073(3) Å). The shorter bond length in the case of aryl stabilisation likely indicates a decrease in dative character and thus an increase in the covalent nature of the Al–C$_{NHC}$ bond (which is also supported by the calculated bond dissociation energy, see below).

Computational discussion of aryl-stabilised dialumene

To gain a deeper insight into the differences between these two classes of dialumenes, we performed density functional theory (DFT) calculations at the B3LYP-D3/6-311G(d) level of theory (for detailed information see the ESI†). The optimised

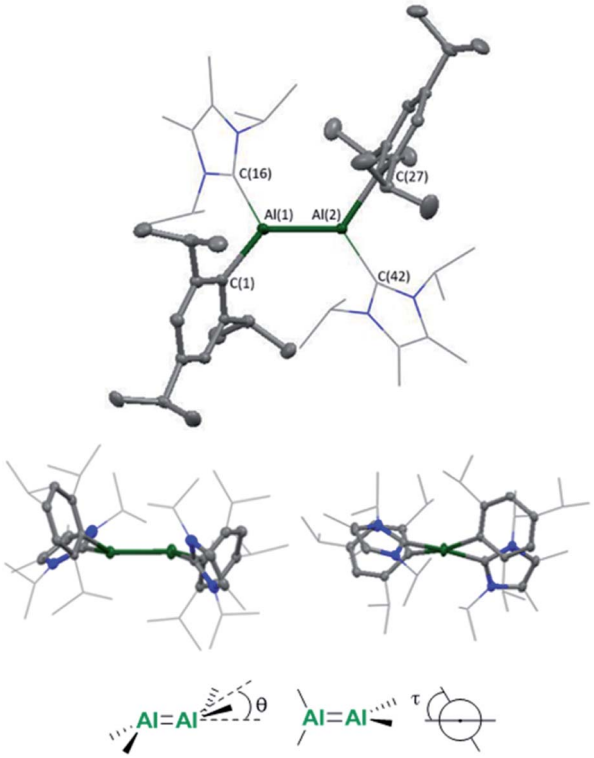

Fig. 1 Molecular structure of compound **3** in the solid state. Ellipsoids are set at the 50% probability level; hydrogen atoms and co-crystallised solvent molecules are omitted for clarity and NHC ligands are depicted in wireframe for simplicity. Selected bond lengths (Å) and angles (°): Al(1)–Al(2) 2.4039(8), Al(1)–C(16) 2.0596(16), Al(2)–C(42) 2.0422(17), Al(1)–C(1) 2.0292(16), Al(2)–C(27) 2.0180(16), C(16)–Al(1)–Al(2) 119.55(5), C(42)–Al(2)–Al(1) 114.13(5), C(1)–Al(1)–Al(2) 123.56(5), C(27)–Al(2)–Al(1) 129.55(5), C(1)–Al(1)–C(16) 110.28(6), C(27)–Al(2)–C(42) 112.84(7), $\theta = 17.25, 23.70$, $\tau = 12.06$.

geometry of **3** is in good agreement with experimental values, with the addition of the dispersion required to account for the *trans*-bent and twisted geometry. For comparison, all calculated values for $\mathbf{3^{Si}}$ including dispersion are given in the ESI.† Analysis of the frontier orbitals of **3** revealed similar features to $\mathbf{3^{Si}}$, in which the HOMO−1 and HOMO contain the Al–Al σ- and π-bonds, respectively, as well as the LUMO representing the Al–C^{NHC} π bond (Fig. 2). The main difference to $\mathbf{3^{Si}}$ (see Fig. S57† for the corresponding orbitals) is the loss of uniform arrangement of the HOMO on the two aluminium centres as well as additional π-incorporation of the NHC present in **3**. We attribute this to the different orientation of the NHCs in **3**, enabling overlap with the p-orbital of the carbene carbon atom, which is experimentally observed as a shortened Al–C^{NHC} bond in the SC-XRD structure and further evidenced by an increased Gibbs free energy of bond dissociation of 26.0 kcal mol^{-1} (*cf.* $\mathbf{3^{Si}}$ = 16.9 kcal mol^{-1}). The conjugation towards the Al–C^{NHC} π-bond in **3** is also observed on inspection of the monomers (for further details see ESI Fig. S62†), which also gives rise to the decreased HOMO–LUMO gap in **3** compared to $\mathbf{3^{Si}}$ (**3** = 1.86 eV, $\mathbf{3^{Si}}$ = 2.24 eV) based on decreased overlap of the monomers being possible.

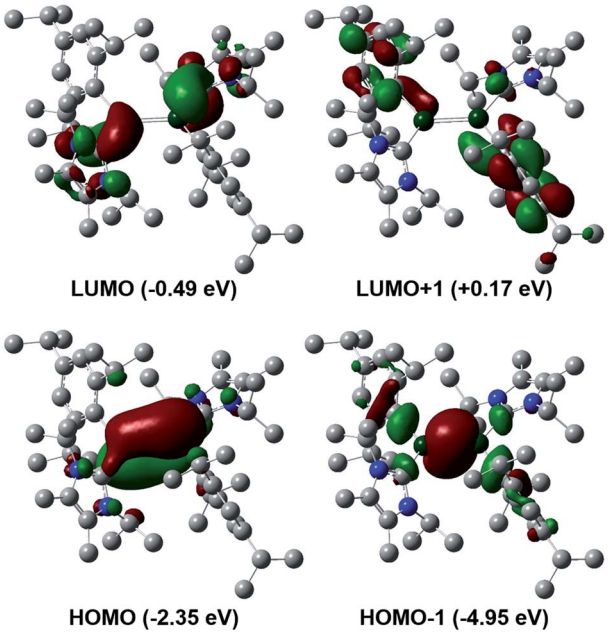

Fig. 2 Frontier orbitals of aryl substituted dialumene **3**.

TD-DFT calculations corroborated the experimental UV/vis spectrum of **3**. This showed an intense absorption band at 833 nm ($\varepsilon = 6273$ L mol^{-1} cm^{-1}) (calc. value 794 nm), which can be assigned to the HOMO to LUMO transition and is responsible for the highly coloured compound.[31] Natural bond orbital (NBO) analysis provided electronic insight into the nature of the Al–Al double bond. The Al–Al π-bond of **3** bears reduced *p*-character compared to $\mathbf{3^{Si}}$. Moreover, this NBO orbital has a lower occupancy based on partial population of the π*-orbitals of the C–N bonds of the NHC, rationalising the increased interaction of the NHC for **3**. This is based on its different orientation, which we mainly attribute to the reduced steric demand of the ligand. Furthermore, this is reflected in the decreased Wiberg bond index (WBI) of the Al–Al bond of 1.67 to 1.53 going from silyl to aryl (Fig. 3), yet still indicating a high degree of multiple bonding character in both systems.

Analysis of NPA charges clearly reflects the silyl effect (Fig. 3): the aluminium centres in $\mathbf{3^{Si}}$ bear a nearly neutral charge of +0.08, while in **3** they account for +0.48/+0.49. We attribute this to the silyl substituents, with their strong σ-donating properties, possessing a more effective orbital overlap with the aluminium centres in the σ(Al–Si) bonds. This also becomes evident upon examination of the results of NBO analysis for the

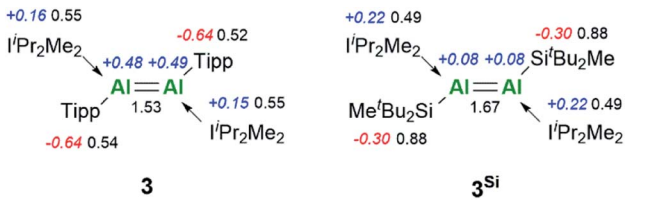

Fig. 3 Results of the NBO analysis of **3** and $\mathbf{3^{Si}}$. NPA charges (blue and red) and WBIs (black).

Al–C^{Tipp}/Al–Si bonds: the Al–C^{Tipp} bonds are highly polarised (17% Al, 83% C^{Tipp}) compared to Al–Si bonds in $\mathbf{3^{Si}}$ (36% Al, 64% Si). This difference is also rationalised upon comparison of Al–C and Al–Si Pauling electronegativities ($\Delta\chi$ Al–C 0.94; $\Delta\chi$ Al–Si 0.29), thus resulting in less polarised Al–Si bonds.

To elucidate the effect of sterics around the aluminium centre, we initially compared the steric demand of the Tipp and Si^{t}Bu$_2$Me ligands, which revealed similar percentages of buried volume (% V_{bur}) of 29.9% (**3**) and 30.7% ($\mathbf{3^{Si}}$) (Fig. S58 and S59†). However, the shape and thus distribution of kinetic stabilisation vary. Further calculation and comparison of reduced model systems were performed with the I^{i}Pr$_2$Me$_2$ carbene replaced by IMe$_4$ ($^{IMe4}\mathbf{3}$ and $^{IMe4}\mathbf{3^{Si}}$, Fig. S60†).[32]

For $^{IMe4}\mathbf{3^{Si}}$ the most stable isomer exhibits a strongly *trans*-bent and twisted geometry ($\theta = 42.1°$, 30.4°, $\tau = 11.7°$) with the NHC planes orientated almost parallel and a substantially elongated Al–Al bond length of 2.43 Å. In the Tipp-substituted $^{IMe4}\mathbf{3}$ the *trans*-bent character is decreased compared to **3**, accompanied by a small increase of the Al–Al bond length due to further rotation of the NHC planes towards the Al–Al plane, enabling more effective π-interaction of NHC and the AlAl moiety. This also becomes more apparent upon examination of the corresponding frontier orbitals with $^{IMe4}\mathbf{3}$. This features enhanced delocalisation of the HOMO onto the NHC moiety, as a consequence of further rotation of the NHC planes towards the Al–Al bond (angle between NHC planes: 49°). In contrast, the HOMO in $^{IMe4}\mathbf{3^{Si}}$ exhibits contributions from the silyl groups, as conjugation towards the NHC π-system is not possible due to the different orientation. Moreover, the HOMO–LUMO gap decreases for aryl and increases for the silyl case, attributed to the decreased/increased *trans*-bent geometry.

The smallest possible model systems, by reducing I^{i}Pr$_2$Me$_2$ to IH$_4$ as well as Tipp/Si^{t}Bu$_2$Me to phenyl/TMS, were calculated and yield comparable results: $^{S}\mathbf{3}$ and $^{S}\mathbf{3^{Si}}$ both possess *trans*-bent but no twisted configuration. In $^{S}\mathbf{3^{Si}}$ a slightly shorter Al–Al bond length and a decreased *trans*-bent angle (21.2° *vs.* 31.8° for $^{S}\mathbf{3}$) are observed; however, in each case the NHC planes are rotated towards the Al═Al bond (see Fig. S61†). Hence, *trans*-bent structures are obtained for the aryl and the silyl substituted dialumenes bearing minimal steric effects. Thus, it is clearly demonstrated that the steric effects of both NHC and the ligands govern the binding motif of dialumenes. The shape of the ligand influences the interaction with the NHC: either only a weak and purely σ-donating type of interaction, as observed in planar $\mathbf{3^{Si}}$, or more flexible coordination of the NHC, with the p-orbital of the $C^{carbene}$ able to form a slipped π-bond with the AlAl core, as observed in **3**. The *trans*-bent and twisted structure obtained for **3** is therefore a result of the difference in steric demand of the Tipp ligand compared to Si^{t}Bu$_2$Me.

From the different aspects, steric as well as electronic, discussed above we thus conclude that the structural difference between **3** and $\mathbf{3^{Si}}$ is caused by the different steric demand of the ligands. From the electronic point of view the change of silyl to Tipp ligand in the dialumene changes the orbital situation at the central AlAl core, which is accompanied by a reduced HOMO–LUMO gap. Moreover, the polarisation of the aluminium centres is different, based on differences in electronegativity between C and Si. We thus anticipate differences in reactivity with respect to activation of strong bonds, such as those in small molecules, as well as an increased accessibility towards a bigger range of reagent molecules of **3**, based on the increased flexibility of this system.

Reactivity of dialumenes

Further differences between these two systems were sought experimentally. Firstly, reactivity towards a series of C–C multiple bonds was examined (Scheme 2). In the case of ethylene, compound **3** underwent formal [2 + 2]-cycloaddition to yield the dialuminacyclobutane compound **4**, akin to the reactivity observed with $\mathbf{3^{Si}}$.[15] Upon reaction with 1 equivalent of phenylacetylene, clean formation of a single species by NMR spectroscopy was noted to occur to form compound **5**. This is in contrast to the reactivity of $\mathbf{3^{Si}}$ where both [2 + 2]-cycloaddition ($\mathbf{5^{Si}}$) and C–H activation were observed. Varying the number of equivalents of phenyl acetylene (2 : 1 and 3 : 1 with respect to **3**) did not result in further incorporation of phenyl acetylene into the complex even at elevated temperatures. However, compound **5** was found to decompose in solution to yield styrene (see ESI Fig. S37 and S38†). Monitoring a C_6D_6 solution of **5** showed that this occurs intramolecularly, with the additional protons required to make styrene likely the result of C–H activation. In further support of an intramolecular C–H activation, addition of a hydrogen source, *e.g.* dihydrogen, phenyl silane, pinacol borane or amine borane, failed to provide any notable increase in the rate of styrene formation. Unfortunately, attempts to identify the fate of the resulting aluminium containing species were unsuccessful. It is proposed that initially [2 + 2]-cycloaddition occurs to form compound **5**, followed by C–H activation of the *iso*-propyl groups of the Tipp ligand, as this was not observed with the analogous silyl complex. Intramolecular C–H activation of the Mes* ligand (Mes* = 2,4,6-tri-*tert*-butylphenyl) has been previously observed by thermolysis of (Mes*)$_2$AlH,[33] whilst 1-germapropadiene, which contains a Ge═C double bond supported by Tipp ligands, also undergoes C–H activation of the Tipp ligand.[34]

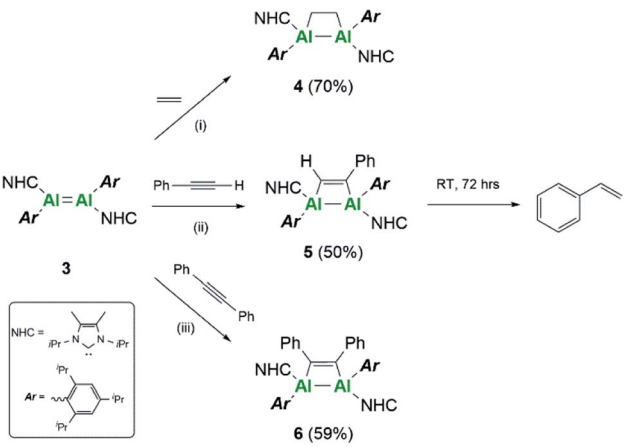

Scheme 2 Reactivity of dialumene (**3**) towards C–C multiple bonds. (i–iii) Toluene, RT, 4 h.

Further reactivity towards C–C multiple bonds was trialed with diphenylacetylene (PhCCPh). Addition of 1 eq. of PhCCPh to $\mathbf{3^{Si}}$ failed to cause a reaction, and after prolonged heating only decomposition of $\mathbf{3^{Si}}$ was observed. In contrast, PhCCPh was observed to react readily with **3**, notably through the instant colour change from the dark black solution of **3** to a yellow solution of compound **6**. This difference in reactivity was surprising, considering that both **3** and $\mathbf{3^{Si}}$ reacted cleanly with both non-polar (ethylene to form **4** and $\mathbf{4^{Si}}$) and polar (phenylacetylene to form **5** and $\mathbf{5^{Si}}$) C–C multiple bonds. This difference in reactivity is thought to be a direct result of the choice of stabilising ligand. The flexibility of the Tipp ligand, due to the rotational *iso*-propyl groups, makes the central AlAl core more accessible for reactant molecules, thus enabling reactivity with more sterically demanding reagents. Moreover, the positive NPA charges of **3** make it more electrophilic in comparison to $\mathbf{3^{Si}}$, thus implying higher reactivity towards nucleophilic C–C multiple bonds.

Compounds **4** and **6** were crystallised from concentrated pentane solutions at −30 °C. The XRD structures revealed addition of the C–C multiple bonds to the dialumene, resulting in the formation of 4-membered rings (Fig. 4). Loss of double bond character from the dialumene was confirmed due to elongation of the Al–Al bond (**4** 2.6035(13), **6** 2.5918(6) *vs.* **3** 2.4039(8) Å). Also noted to occur is the elongation of the Al–C^{NHC} bond lengths (**4** 2.079(3), 2.093(3), **6** 2.1097(15) *vs.* **3** 2.0596(16), 2.0422(17) Å). The 4-membered ring in **6** is almost planar (6.37° between Al–Al–C(27) planes), whilst **4** is puckered due to the presence of the sp^3 carbons.

Extension of this work towards C–N triple bonds focused on the use of 2,6-dimethylphenylisocyanide (XylNC). Previously, Tokitoh and co-workers had shown that reaction of their masked dialumene species resulted in homocoupling of isocyanides.[35] Reactions of varying equivalents of XylNC to $\mathbf{3^{Si}}$ all resulted in an ill-defined mixture of species; unfortunately, attempts to separate species through fractional crystallisation failed. In contrast, reaction of 2 eq. of XylNC with **3** resulted in a clear colour change from black to red and produced a well-defined but complex ^{1}H NMR spectrum of compound **7** (Scheme 3). This complex contains bridging CNXyl units due to the observed downfield signal in the ^{13}C NMR spectrum at δ 303.4 ppm. This was similar to the previously observed bridging carbonyl fragment observed with $\mathbf{3^{Si}}$, in the rearrangement of CO_2 (δ 276.0 ppm)[16] and the bridging isocyanide intermediate reported by Tokitoh (δ 294.7 ppm).[35] Single crystals of **7** were grown from a 2 : 1 (toluene : hexane) mixture at 5 °C, revealing a butterfly configuration with two μ-CNXyl units (Fig. 5).

The central Al–C^{Xyl}–Al–C^{Xyl} core in compound **7** is puckered (34.3° between the two C^{Xyl}–Al–C^{Xyl} planes), with the supporting NHC and Tipp ligands now *cis* to the ring. This change from *trans* to *cis*-conformation has been observed previously for the C–H activated phenylacetylene product on reaction with $\mathbf{3^{Si}}$. However, the reasons for such a change in conformation are unclear. Again, elongation of the Al–C^{NHC} bond lengths are observed (Al–C^{NHC} 2.109(3) Å), with the change in Al–C^{Tipp} negligible (**7** 2.042(7) *vs.* **3** (2.0292(16) Å). Reduction of the C–N triple bond to a double bond is confirmed on inspection of the bond length (C(27)–N(3) 1.292(4) Å), which is in line with average C=N bond lengths.[36–39] Additionally, the change in angle around the nitrogen in XylNC from linear to bent (126.3 (2) °) confirms reduction of the C–N triple bond. This butterfly configuration has been previously observed with transition metal complexes;[40–47] however, they all contain a M–M bond, and those without M–M bonds contain a planar central ring.[48–52]

To confirm the nature of the bonding within compound **7** DFT studies were performed again, at the B3LYP-D3/6-311G(d) level of theory. The optimised structure is in good agreement with the one obtained experimentally by SC-XRD, including the calculated C=N IR stretching frequencies (experimental: 1545 cm^{-1} *vs.* calculated: 1568 cm^{-1}). Orbital analysis (Fig. 6)

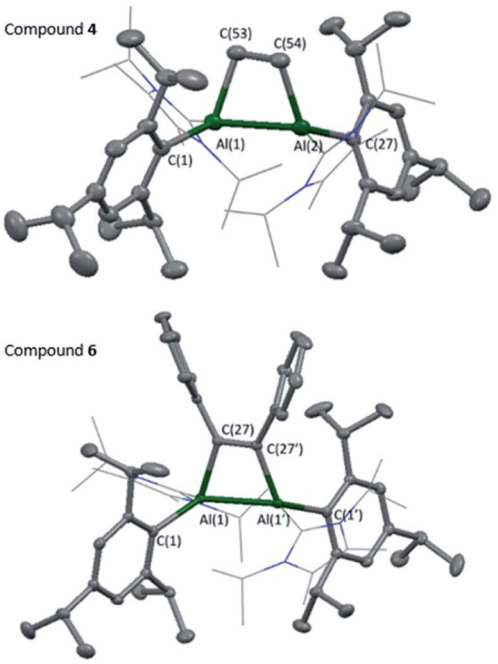

Fig. 4 Molecular structures of compounds **4** and **6** in the solid state. Ellipsoids are set at the 50% probability level; hydrogen atoms and co-crystallised solvent molecules are omitted for clarity and NHC ligands are depicted in wireframe for simplicity. Selected bond lengths (Å) and angles (°): **4**: Al(1)–Al(2) 2.6035(13), Al(1)–C(1) 2.053(3), Al(1)–C(16) 2.079(3), Al(1)–C(53) 2.052(3), C(53)–C(54) 1.565(5), Al(2)–C(27) 2.048(3), Al(2)–C(42) 2.093(3), Al(2)–C(54) 2.040(3), Al(1)–Al(2)–C(54) 73.50(11), Al(2)–Al(1)–C(53) 72.94(11), C(54)–C(53)–Al(1) 101.33(19), C(53)–C(54)–Al(2) 101.23(19). **6**: Al(1)–Al(1′) 2.5918(6), Al(1)–C(1) 2.0413(14), Al(1)–C(16) 2.1097(15), Al(1)–C(27) 2.0246(14), C(27)–C(27′) 1.3701(19), Al(1′)–Al(1)–C(27) 72.19(4), Al(1)–C(27)–C(27′) 107.09(10).

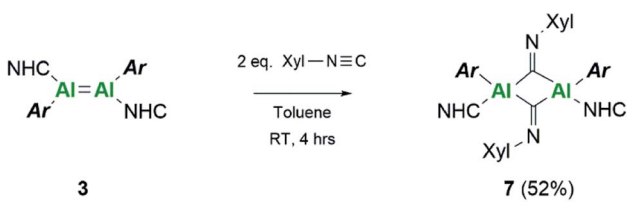

Scheme 3 Reactivity of dialumene (**3**) towards isocyanide.

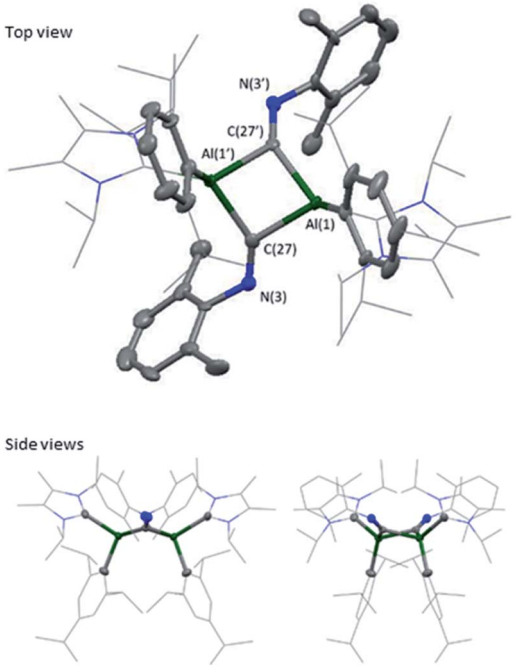

Fig. 5 Molecular structure of compound **7** in the solid state. Ellipsoids are set at the 50% probability level; hydrogen atoms and co-crystallised solvent molecules are omitted for clarity and NHC ligands and iso-propyl groups are depicted in wireframe for simplicity. Selected bond lengths (Å) and angles (°): Al(1)–C(1) 2.042(7), Al(1)–C(16) 2.109(3), Al(1)–C(27) 2.059(3), C(27)–N(3) 1.292(4), Al(1)–C(27)–Al(1′) 91.59(11), C(27)–Al(1)–C(27′) 82.74(11), C(27)–N(3)–C(28) 126.3(2).

revealed the HOMO as an orbital overlap of aluminium and π*(C–N). The LUMO represents the combination perpendicular to the HOMO, including conjugation across the central ring. NBO calculations confirmed that no C–C or Al–Al bond is present in **7** (WBI ($C^{27}C^{27'}$):0.06; WBI ($Al^{1}Al^{1'}$): 0.04).

Small molecule activation

Further reactivity differences were sought through investigation towards small molecules (Scheme 4). Previously, reaction of $\mathbf{3^{Si}}$ towards carbon dioxide (CO_2) resulted in an initial CO_2 fixation complex.[16] This subsequently underwent C–O cleavage reaction, in the absence of additional CO_2 through rearrangement to a bridging carbonyl complex, whilst in the presence of CO_2, formation of a carbonate species with elimination of CO was observed. On reaction of **3** with CO_2 immediate loss of the black

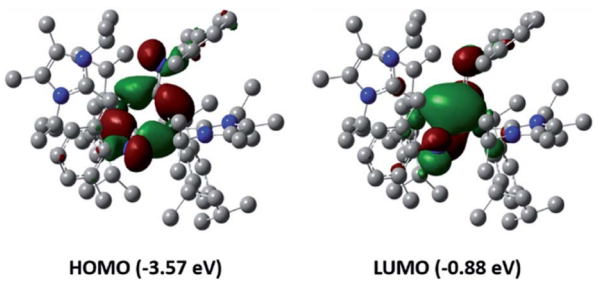

Fig. 6 Frontier orbitals of compound **7**.

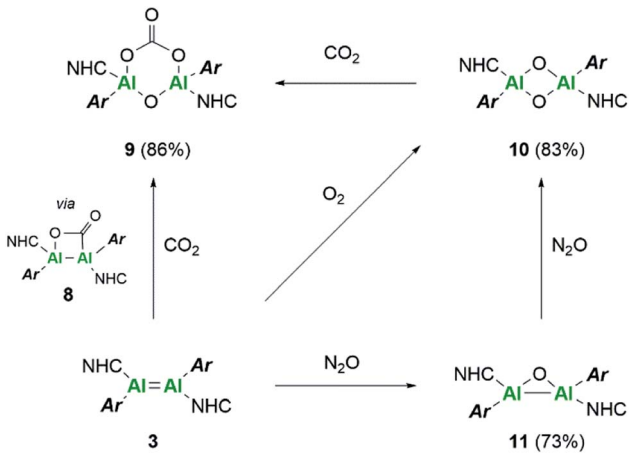

Scheme 4 Reactivity of dialumene (**3**) towards small molecules, CO_2, O_2 and N_2O.

colour and formation of a colourless solution was observed. On inspection of the ^{13}C NMR spectrum, the presence of CO (δ 184.4 ppm) and CO_3 (δ 159.12 ppm) was observed, indicating the formation of the carbonate complex compound **9**. In contrast to $\mathbf{3^{Si}}$, attempts to isolate the CO_2 fixation product were unsuccessful as it rapidly converted to compound **9**. Use of the labile $I^{i}Pr_2Me_2$–CO_2 species allowed for the formal [2 + 2]-cycloaddition product (compound **8**) to be observed due to its characteristic ^{13}C resonance at δ 207.7 ppm ($\mathbf{8^{Si}}$ δ 209.9 ppm). However, this reaction resulted in multiple species as well as compound **9**, owing to the higher reactivity of the Tipp dialumene (compound **3**), thus indicating that formation of **9** proceeds through the CO_2 fixation species in a similar manner to $\mathbf{3^{Si}}$.

Reaction of **3** with O_2 resulted in the expected dioxo product, compound **10**, same as the previously reported reaction of $\mathbf{3^{Si}}$. In a similar manner to $\mathbf{10^{Si}}$, compound **10** can also be reacted with CO_2 resulting in carbonate complex **9**. In a notable difference to the silyl supported reactivity, addition of N_2O to compound **3** resulted in a dark red solution at room temperature ($\mathbf{3^{Si}}$ yielded colourless compound $\mathbf{10^{Si}}$). This red solution was observed to slowly fade to colourless over a few hours and the formation of compound **10** was confirmed by ^{1}H NMR spectroscopy. Use of 1 eq. of an oxygen donor reagent, namely *N*-methylmorpholine-*N*-oxide, with **3** allowed for clean isolation of the red species, compound **11**. Compound **11** is stable in the solid state for up to two months in a glovebox freezer; however, at room temperature and in solution, further oxidation to compound **10** occurs. Whilst ^{1}H NMR showed similar environments for both **10** and **11** (Fig. S39†), compound **11** is intensely coloured (UV/vis = 512 nm, $\varepsilon = 1155$ L mol^{-1} cm^{-1}) whilst **10** is colourless. As such compound **11** was tentatively assigned as a bridging aluminium(II) mono-oxide species, rather than a terminal aluminium(III) mono-oxide complex. Unfortunately, SC-XRD analysis did not provide clear structural parameters for the mono-oxide species due to superposition with compound **10** (Fig. S55†). To provide further insight, calculations were also performed on compounds **10** and **11**. The optimised structure

of **10** is symmetric relating to the Al–O bonds, as previously observed for the analogous silyl compound (**10**^{Si}).[16] TD-DFT calculations revealed the highest transition at 259 nm, in line with the experimental colourless appearance. In contrast, compound **11** bears substantial π-electron density between the two aluminium centres in the HOMO as depicted in Fig. 7, reminiscent of the disilaoxirane reported by our group.[53] The LUMO represents the unoccupied π(Al–C^{NHC}) bond. TD-DFT calculations verified the experimentally observed red colour (UV-vis 512 nm) with good accordance (calc. 519 nm), assigned to the HOMO to LUMO transitions of **11**.

Extension of this small molecule reactivity towards dihydrogen was investigated. Firstly, a J-Young NMR tube containing a purple solution of **3**^{Si} was freeze–pump–thaw degassed and then backfilled with approximately 1 atm of H_2. After 24 hours at room temperature no reaction was noted to have occurred; increasing the temperature to 60 °C and regular monitoring only resulted in the observed decomposition of **3**^{Si}.

Repetition of this reaction with the aryl stabilised dialumene, compound **3**, also resulted in no reaction at room temperature. After 16 h at 50 °C, however, the black colour of **3** had faded to a dark brown/yellow solution (Scheme 5). On inspection of the ^{1}H NMR spectrum, no Al–H signals could be observed owing to the quadrupolar nature of the Al centre. Additionally, three distinct *iso*-propyl signals similar to that observed for compound **1** were identified. These, however, were not identical and therefore complete hydrogenation and cleavage of the Al–Al bond can be ruled out. Thus, it is likely that compound **12** consists of either terminal or bridging hydrides.

IR spectroscopy was utilised to differentiate between the two likely structures; two broad but distinct peaks at 1593 and 1634 cm^{-1} were observed. Compounds containing no Al–Al bond but both terminal and bridging hydrides are found at approximately 1880 cm^{-1} and 1350 cm^{-1}, respectively,[20,54] whilst terminal hydrides within complexes containing Al–Al bonds are found within 1680–1835 cm^{-1},[55] thus pointing more in the direction of a terminal hydride with Al–Al bonds. Additionally, for the previous terminal hydride in the related silyl system, from C–H activation of phenyl acetylene, this Al–H was found at 1666 cm^{-1}.[15] Unfortunately, attempts to grow crystals suitable for SC-XRD were unsuccessful. Therefore, additional insight for this structure was sought computationally. Different possible isomers of product **12** were calculated, including bridging, terminal, and combinations of both as well as different rotational isomers (H: *cis* or *trans*; NHC and Tipp ligands: *cis* or *trans*).

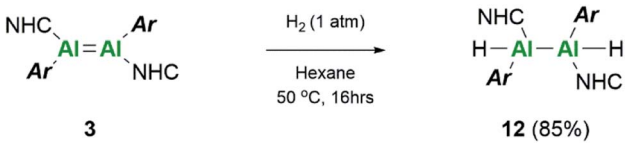

Scheme 5 Reactivity of dialumene (**3**) towards dihydrogen.

The two lowest lying isomers were found to possess terminal hydrides in the *cis* and *trans* configurations (Fig. 8). The Al–H stretching frequencies were calculated to be 1634 and 1676 cm^{-1}, respectively, which is in good agreement with the experimentally obtained values (for detailed information see the ESI†). It is, therefore, suggested that the activation of hydrogen by **3** results in both the *cis* and *trans* isomers of compound **12**.

Catalysis

Further comparisons between the two dialumenes examined their use in catalytic applications. Two archetypal catalytic reactions (hydroboration and dehydrocoupling) were studied due to their prevalence in main group catalysis, as well as the implication of metal-hydrides in facilitating turnover.[56,57] With the ability to form dialuminium-hydrides in the case of **3** and not for **3**^{Si}, differences in activity and mechanistic pathways are anticipated.

CO_2 hydroboration

Previously, **3**^{Si} was found to selectively catalyse the reduction of CO_2 to a formic acid equivalent (product **A**, Scheme 6) with

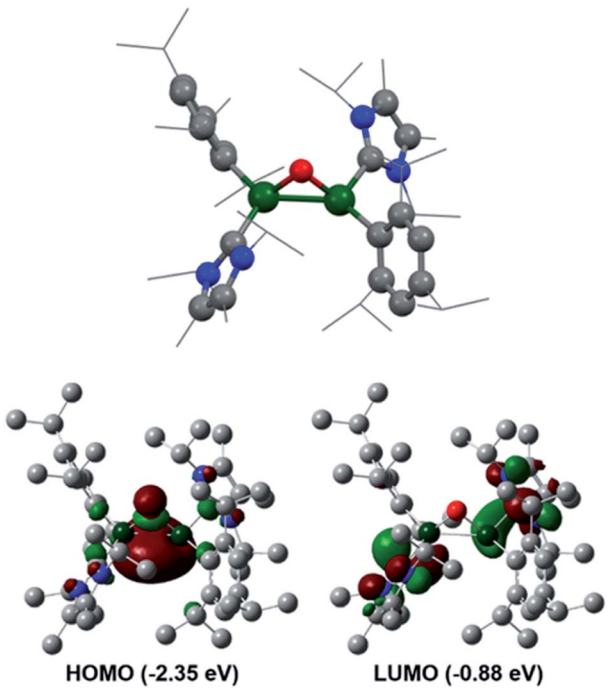

Fig. 7 Calculated molecular structure of compound **11** and its frontier orbitals.

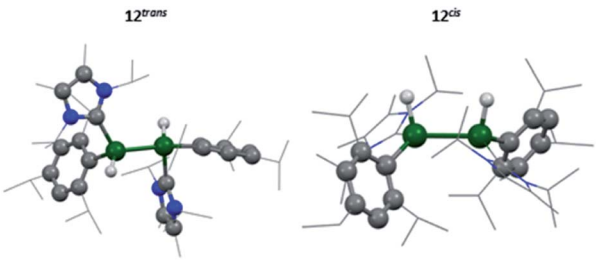

Fig. 8 Calculated molecular structure of **12**^{trans}/**12**^{cis}.

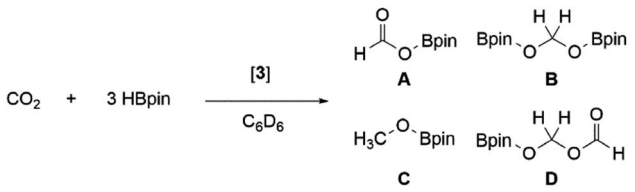

Scheme 6 Catalytic hydroboration of CO_2 mediated by dialumene (**3**).

pinacol borane (HBpin).[16] Whilst this reaction does proceed at room temperature, it required up to 1 week and 10 mol% of $\mathbf{3^{Si}}$ (Table 1, entry 1); use of higher temperatures allowed for reduced catalyst loadings and decreased reaction times (Table 1, entry 2). As **3** has so far shown increased reactivity, a trial reaction with 5 mol% of **3** towards hydroboration of CO_2 at room temperature was carried out (Table 1, entry 3). On regular monitoring through ^{1}H and ^{11}B NMR spectroscopy the consumption of HBpin was noted to occur along with the formation of new B–O containing species. The corresponding ^{1}H NMR spectrum showed the presence of further reduced species (**A–D**, Scheme 6), indicating that **3** is not only more catalytically active, but also proceeds through an alternate mechanism due to the presence of **B–C**.

Again, through use of a higher temperature (60 °C), the catalyst loading could be decreased down to 1 mol% (Table 1, entry 5). This resulted in the same consumption of HBpin after 24 h (at RT) as with 5 mol% (Table 1, entry 4); however, the resulting product distribution differs, with higher temperatures favouring the formation of the triply reduced methanol equivalent (product **C**, Scheme 6).

The formation of more highly reduced species indicates a likely change in the mechanism. Previously, $\mathbf{3^{Si}}$ showed no reactivity towards HBpin and as such a non-hydridic mechanism based on the initial formation of $\mathbf{9^{Si}}$ was proposed. From computational analysis, coordination of HBpin and subsequent reduction of the exocyclic carbonyl of $\mathbf{9^{Si}}$ was found to be rate determining. Turnover was achieved through coordination/insertion of an additional CO_2 on the opposite side of the Al···Al plane resulting in formation of an 8-membered ring which collapses to reform $\mathbf{9^{Si}}$ with release of the formic acid equivalent. This mechanism also further supports the observed selectivity towards product **A**.[16]

In this instance, use of **3** results in the formation of products **B–D** in notable amounts; therefore, an alternative mechanism for the hydroboration of CO_2 is highly likely. As such, **3** was reacted with 1 eq. of HBpin; the ^{11}B NMR spectrum showed complete consumption of HBpin and formation of a new upfield doublet at δ 2.57 ppm (J_{HB} = 112.18 Hz). The same signal and coupling were observed from the reaction of HBpin and $I^iPr_2Me_2$; therefore it is proposed that the stoichiometric reaction of **3** and HBpin results in NHC abstraction. Notably, this does not result in H–B bond cleavage and formation of an Al(H)–Al(Bpin) type species, which was observed with diborene[58] and disilyne[59] chemistry. Addition of CO_2 to this $I^iPr_2Me_2$–HBpin adduct did not result in formation of any reduced CO_2 species, or any reaction after 24 h at room temperature; therefore it is unlikely that this is the catalytically active species. It is of note that NHCs have been shown to catalyse hydroboration (with HBpin) of carbonyl compounds, in acetonitrile.[60]

Whilst these experimental observations preclude definitive mechanistic analysis, it is proposed that the aryl stabilised dialumene (**3**) acts as a pre-catalyst, with CO_2 hydroboration occurring through an initial hydroalumination of CO_2 and subsequent Al–O/B–H σ-bond metathesis, in line with other previously reported main group hydroelementation of CO_2 mechanisms.[61–70]

Amine borane dehydrogenation

Main group catalysts (largely group 1, 2, and 13) have also been shown to be viable dehydrocoupling catalysts.[56,57,71,72] These reactions largely proceed through formation of M–H and M–E

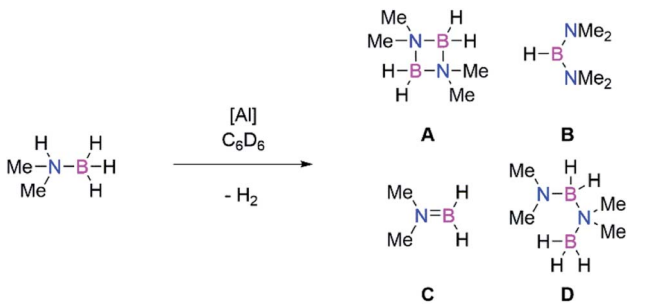

Scheme 7 Catalytic dehydrocoupling of Me_2NHBH_3 mediated by aluminium catalysts.

Table 1 Catalytic hydroboration of CO_2 by dialumenes (**3** and $\mathbf{3^{Si}}$)

						Product distribution[b]/%			
Entry	Catalyst	Loading/mol%	Time/h	Temp/°C	Conversion[a]/%	**A**	**B**	**C**	**D**
1	$\mathbf{3^{Si}}$	10	110	20	86	86	7	7	0
2	$\mathbf{3^{Si}}$	5	4	60	68	94	2	4	0
3	**3**	5	58	20	81	39	27	34	0
4	**3**	5	24	20	66	65	15	17	3
5	**3**	1	24	60	62	49	7	41	3

[a] Conversion of HBpin based on ^{11}B NMR integrals. [b] Ratio of products based on ^{1}H NMR integrals.

Table 2 Catalytic dehydrocoupling of Me_2NHBH_3 by aluminium catalysts

Entry	Catalyst	Loading/mol%	Time/hr	Temp/°C	Conversion[a]/%	Product distribution[b]/%			
						A	**B**	**C**	**D**
1	**3**	5	5	20	72	25	5	—	27
2	**3**	5	44	20	78	35	5	—	23
3	$\mathbf{3^{Si}}$	5	16.5	20	17	5	1	—	11
4	**3**	1	2	20	28	8	1	<1	13
5	**3**	1	16.5	20	60	45	1	<1	14
6	**1**	5	24	20	0	0	0	0	0
7	**1**	5	24	60	31	11	—	—	15

[a] Conversion of Me_2NHBH_3 based on ^{11}B NMR integrals. [b] Ratio of products based on ^{11}B NMR integrals.

bonds, *via* σ-bond metathesis reactions due to the differing protic and hydridic substrates. Therefore, to probe the intermediacy of aluminium hydrides we examined the use of both dialumenes in amine-borane dehydrocoupling catalysis. Use of 5 mol% of **3** and $\mathbf{3^{Si}}$ with Me_2NHBH_3 in C_6D_6 showed rapid evolution of gas at room temperature in the case of the aryl substituted dialumene (**3**). Regular monitoring of both reaction mixtures at room temperature by ^1H and ^{11}B NMR spectroscopy confirmed the formation of H_2 and showed several boron containing species by ^{11}B NMR (Scheme 7, products **A–D**). After 5 h approximately 70% of the Me_2NHBH_3 had been consumed in the case of **3** (Table 2, entry 1); in contrast, the silyl dialumene $\mathbf{3^{Si}}$ after three times as long resulted in 17% consumption of Me_2NHBH_3 (Table 2, entry 3). Notably, prolonged reaction times in the case of the **3** did not lead to significant or complete consumption of Me_2NHBH_3 (Table 2, entry 2), and only a small change in the product distribution was observed with increased reaction times.

It was also possible to use 1 mol% of **3**; again, fast consumption of Me_2NHBH_3 was observed within the first few hours (Table 2, entry 4) with the reaction rate slowing with increased Me_2NHBH_3 consumption (Table 2, entry 5). As aluminium-hydrides have been used in amine borane catalysis previously,[73] and to rule out complete hydrogenation and Al–Al bond cleavage during the reaction, compound **1** was tested for dehydrocoupling activity. After 24 h at room temperature (Table 2, entry 6) no conversion of Me_2NHBH_3 was observed; on increasing the temperature to 60 °C (Table 2, entry 7), some formation of H_2 and products **A–D** was observed. Due to the increased temperature and prolonged reaction times required for compound **1**, it is proposed that the retention of an Al–Al bond accounts for the increased catalytic activity.

Comparable to hydroboration reactions, the aryl stabilised dialumene (**3**) was found to be more catalytically active than the silyl-stabilised counterpart ($\mathbf{3^{Si}}$). Mechanistically speaking, amine-borane dehydrocoupling reactions generally occur through formation of M–H and M–E bonds.[57] As such, it has been shown that formation of Al–H bonds is more accessible from **3** compared to $\mathbf{3^{Si}}$, therefore accounting for the difference in catalytic activity. Both reactions show initial formation of a catalytic equivalent of $HB(NMe_2)_2$ (product **B**, Scheme 7) which then remains constant throughout the catalysis. It has previously been shown by Wright and co-workers that formation of **B** is the result of the formation of the catalytically active Al–H containing species from $Al(NR_3)_3$ (R = Me, iPr).[74] Furthermore, Braunschweig and co-workers recently showed that Me_2NHBH_3 can be used to isolate hydrogenated diborenes; thus, analogous reactivity is anticipated.[75] However, in our hands, stoichiometric reactions of **3** and Me_2NHBH_3 resulted in a mixture of species, whilst reaction with a higher number of equivalents of Me_2NHBH_3 resulted in the dehydrocoupling products. We therefore conclude that the dialumene acts as a pre-catalyst in this reaction and the active catalyst is generated *in situ*.

Conclusions

In conclusion, we have shown the fundamental differences between aryl and silyl supporting ligands for the stabilisation of dialumenes and their subsequent influence on reactivity. The increased flexibility of the *trans*-bent and twisted structure for the aryl dialumene (**3**) enables reactivity with more sterically demanding substrates, and in addition is now able to activate dihydrogen. Further differences are observed in the catalytic ability of the two dialumenes, with the latter exhibiting higher activity. This is likely due to different mechanisms in the catalytic cycle and the ability of the aryl dialumene to stabilise a metal-hydride intermediate in contrast to the silyl ligand.

Conflicts of interest

There are no conflicts to declare.

Acknowledgements

We thank Prof. Dr M. C. Holthausen and Dr J. I. Schweizer (Goethe-Universität Frankfurt am Main) for fruitful discussions, computational resources, and advice. Quantum chemical calculations were performed in parts at the Leibniz Supercomputing Center of the Bavarian Academy of Science and Humanities. We are also grateful to Dr A. Pöthig and Dr C. Jandl for crystallographic advice, and M. Muhr (Prof. R. A. Fischer, TUM) for the LIFDI-MS measurements. This project has received funding from the European Union's Horizon 2020 research and innovation program under the Marie Skłodowska-

Curie grant agreement No 754462 (Fellowship CW), as well as the European Research Council (SILION 637394) and WACKER Chemie AG.

Notes and references

1 F. A. Cotton, C. A. Murillo and R. A. Walton, *Multiple Bonds Between Metal Atoms*, Springer, New York, 3rd edn, 2005.
2 R. West, M. J. Fink and J. Michl, *Science*, 1981, **214**, 1343.
3 P. J. Davidson and M. F. Lappert, *J. Chem. Soc., Chem. Commun.*, 1973, 317a.
4 A. G. Brook, F. Abdesaken, B. Gutekunst, G. Gutekunst and R. K. Kallury, *J. Chem. Soc., Chem. Commun.*, 1981, 191–192.
5 M. Yoshifuji, I. Shima, N. Inamoto, K. Hirotsu and T. J. Higuchi, *J. Am. Chem. Soc.*, 1981, **103**, 4587–4589.
6 P. P. Power, *Chem. Rev.*, 1999, **99**, 3463–3504.
7 R. C. Fischer and P. P. Power, *Chem. Rev.*, 2010, **110**, 3877–3923.
8 P. P. Power, *Nature*, 2010, **463**, 171–177.
9 C. Weetman and S. Inoue, *ChemCatChem*, 2018, **10**, 4213–4228.
10 R. L. Melen, *Science*, 2019, **363**, 479–484.
11 G. H. Spikes, J. C. Fettinger and P. P. Power, *J. Am. Chem. Soc.*, 2005, **127**, 12232–12233.
12 M. Kira, S. Ohya, T. Iwamoto, M. Ichinohe and C. Kabuto, *Organometallics*, 2000, **19**, 1817–1819.
13 M. Kira, *Proc. Jpn. Acad., Ser. B*, 2012, **88**, 167–191.
14 D. Wendel, T. Szilvási, C. Jandl, S. Inoue and B. Rieger, *J. Am. Chem. Soc.*, 2017, **139**, 9156–9159.
15 P. Bag, A. Porzelt, P. J. Altmann and S. Inoue, *J. Am. Chem. Soc.*, 2017, **139**, 14384–14387.
16 C. Weetman, P. Bag, T. Silvási, C. Jandl and S. Inoue, *Angew. Chem., Int. Ed.*, 2019, **58**, 10961–10965.
17 P. Bag, C. Weetman and S. Inoue, *Angew. Chem., Int. Ed.*, 2018, **57**, 14394–14413.
18 R. J. Wright, A. D. Phillips and P. P. Power, *J. Am. Chem. Soc.*, 2003, **125**, 10784–10785.
19 T. Agou, K. Nagata and N. Tokitoh, *Angew. Chem., Int. Ed.*, 2013, **52**, 10818–10821.
20 K. Nagata, T. Murosaki, T. Agou, T. Sasamori, T. Matsuo and N. Tokitoh, *Angew. Chem., Int. Ed.*, 2016, **55**, 12877–12880.
21 N. J. Hardman, R. J. Wright, A. D. Phillips and P. P. Power, *J. Am. Chem. Soc.*, 2003, **125**, 2667–2679.
22 Z. Zhu, R. C. Fischer, B. D. Ellis, E. Rivard, W. A. Merrill, M. M. Olmstead, P. P. Power, J. D. Guo, S. Nagase and L. Pu, *Chem.–Eur. J.*, 2009, **15**, 5263–5272.
23 R. J. Wright, A. D. Phillips, S. Hino and P. P. Power, *J. Am. Chem. Soc.*, 2005, **127**, 4794–4799.
24 E. Rivard and P. P. Power, *Inorg. Chem.*, 2007, **46**, 10047–10064.
25 J. Moilanen, P. P. Power and H. M. Tuononen, *Inorg. Chem.*, 2010, **49**, 10992–11000.
26 C. A. Caputo, J.-D. Guo, S. Nagase, J. C. Fettinger and P. P. Power, *J. Am. Chem. Soc.*, 2012, **134**, 7155–7164.
27 C. A. Caputo, J. Koivistoinen, J. Moilanen, J. N. Boynton, H. M. Tuononen and P. P. Power, *J. Am. Chem. Soc.*, 2013, **135**, 1952–1960.
28 C. A. Caputo and P. P. Power, *Organometallics*, 2013, **32**, 2278–2286.
29 Attempts to follow a similar synthetic strategy to the previous dihalide precursor, *i.e.* halogenation followed by salt metathesis with LiTipp, resulted in a largely unreacted mixture after 36 hrs at room temperature with 10% conversion to a mixture of compounds which could not be separated.
30 P. Pyykkö and M. Atsumi, *Chem.–Eur. J.*, 2009, **15**, 186–197.
31 Compared to $\mathbf{3^{Si}}$, mixing of the π(Al–Al) and π*(C^{NHC}–N) raises the HOMO energy, with the HOMO to LUMO transition shifted to higher wavelength in the UV-vis spectrum. Several smaller absorptions, only observable as a broad band around 600 nm (see Table S4†), are attributed to HOMO to LUMO+1/+3 transitions.
32 Experimental attempts to isolate an IMe_4 stabilised dialumene failed in both silyl and Tipp based systems. This was trialed both through analogous synthetic procedures and ligand exchange reactions on the isolated complexes **3** and $\mathbf{3^{Si}}$.
33 R. J. Wehmschulte and P. P. Power, *Inorg. Chem.*, 1998, **37**, 2106–2109.
34 B. E. Eichler, D. R. Powell and R. West, *Organometallics*, 1999, **18**, 540–545.
35 K. Nagata, T. Agou, T. Sasamori and N. Tokitoh, *Chem. Lett.*, 2015, **44**, 1610–1612.
36 C. Weetman, M. S. Hill and M. F. Mahon, *Chem. Commun.*, 2015, **51**, 14477–14480.
37 W. Uhl and M. Matar, *Z. Naturforsch., B: Chem. Sci.*, 2004, **59**, 1214–1222.
38 R. Lalrempuia, C. E. Kefalidis, S. J. Bonyhady, B. Schwarze, L. Maron, A. Stasch and C. Jones, *J. Am. Chem. Soc.*, 2015, **137**, 8944–8947.
39 J. Spielmann and S. Harder, *Chem.–Eur. J.*, 2007, **13**, 8928–8938.
40 R. C. Pettersen and G. G. Cash, *Acta Crystallogr., Sect. B: Struct. Crystallogr. Cryst. Chem.*, 1977, **33**, 2331–2334.
41 F. A. Cotton and B. A. Frenz, *Inorg. Chem.*, 1974, **13**, 253–256.
42 R. D. Adams, F. A. Cotton and G. A. Rusholme, *J. Coord. Chem.*, 1972, **1**, 275–283.
43 W. E. Carroll, M. Green, A. M. R. Galas, M. Murray, T. W. Turney, A. J. Welch and P. Woodward, *J. Chem. Soc., Dalton Trans.*, 1980, 80–86.
44 T. Takao, N. Obayashi, B. Zhao, K. Akiyoshi, H. Omori and H. Suzuki, *Organometallics*, 2011, **30**, 5057–5067.
45 G. Cox, C. Dowling, A. R. Manning, P. McArdle and D. Cunningham, *J. Organomet. Chem.*, 1992, **438**, 143–158.
46 K. Boss, C. Dowling, A. R. Manning, D. Cunningham and P. McArdle, *J. Organomet. Chem.*, 1999, **579**, 252–268.
47 A. R. Manning, K. Boss, M. G. Cox, A. McCabe, P. Soye, S. C. Wade, P. A. McArdle and D. Cunningham, *J. Organomet. Chem.*, 1995, **487**, 151–162.
48 M. Weidenbruch, B. Brand-Roth, S. Pohl and W. Saak, *Angew. Chem., Int. Ed.*, 1990, **29**, 90–92.
49 M. Weidenbruch, J. Hamann, H. Piel, D. Lentz, K. Peters and H. G. von Schnering, *J. Organomet. Chem.*, 1992, **426**, 35–40.

50 D. Lentz, I. Brüdgam and H. Hartl, *J. Organomet. Chem.*, 1986, **299**, C38–C42.
51 D. Lentz and S. Willemsen, *J. Organomet. Chem.*, 2000, **612**, 96–105.
52 A. K. Adhikari, M. B. Sárosi, T. Grell, P. Lönnecke and E. Hey-Hawkins, *Chem.–Eur. J.*, 2016, **22**, 15664–15668.
53 D. Wendel, T. Szilvási, D. Henschel, P. J. Altmann, C. Jandl, S. Inoue and B. Rieger, *Angew. Chem., Int. Ed.*, 2018, **57**, 14575–14579.
54 R. J. Wehmschulte and P. P. Power, *Inorg. Chem.*, 1994, **33**, 5611–5612.
55 S. J. Bonyhady, D. Collis, G. Frenking, N. Holzmann, C. Jones and A. Stasch, *Nat. Chem.*, 2010, **2**(10), 865–869.
56 M. S. Hill, D. J. Liptrot and C. Weetman, *Chem. Soc. Rev.*, 2016, **45**, 972–988.
57 R. L. Melen, *Chem. Soc. Rev.*, 2016, **45**, 775–788.
58 H. Braunschweig, R. D. Dewhurst, C. Hörl, A. K. Phukan, F. Pinzner and S. Ullrich, *Angew. Chem., Int. Ed.*, 2014, **53**, 3241–3244.
59 K. Takeuchi, M. Ikoshi, M. Ichinohe and A. Sekiguchi, *J. Am. Chem. Soc.*, 2010, **132**, 930–931.
60 T. Li, J. Zhang and C. Cui, *Chin. J. Chem.*, 2019, **37**, 679–683.
61 A. Caise, D. Jones, E. L. Kolychev, J. Hicks, J. M. Goicoechea and S. Aldridge, *Chem.–Eur. J.*, 2018, **24**, 13624–13635.
62 D. Franz, C. Jandl, C. Stark and S. Inoue, *ChemCatChem*, 2019, **11**, 5275–5281.
63 M. D. Anker, M. Arrowsmith, P. Bellham, M. S. Hill, G. Kociok-Köhn, D. J. Liptrot, M. F. Mahon and C. Weetman, *Chem. Sci.*, 2014, **5**, 2826–2830.
64 G. Tan, W. Wang, B. Blom and M. Driess, *Dalton Trans.*, 2014, **43**, 6006–6011.
65 D. Mukherjee, S. Shirase, T. P. Spaniol, K. Mashima and J. Okuda, *Chem. Commun.*, 2016, **52**, 13155–13158.
66 D. Mukherjee, H. Osseili, T. P. Spaniol and J. Okuda, *J. Am. Chem. Soc.*, 2016, **138**, 10790–10793.
67 A. Jana, D. Ghoshal, H. W. Roesky, I. Objartel, G. Schwab and D. Stalke, *J. Am. Chem. Soc.*, 2009, **131**, 1288–1293.
68 T. J. Hadlington, C. E. Kefalidis, L. Maron and C. Jones, *ACS Catal.*, 2017, **7**, 1853–1859.
69 J. A. Abdalla, I. M. Riddlestone, R. Tirfoin and S. Aldridge, *Angew. Chem., Int. Ed.*, 2015, **54**, 5098–5102.
70 A. Jana, G. Tavčar, H. W. Roesky and M. John, *Dalton Trans.*, 2010, **39**, 9487–9489.
71 R. J. Less, R. L. Melen and D. S. Wright, *RSC Adv.*, 2012, **2**, 2191–2199.
72 J. D. Erickson, T. Yi Lai, D. J. Liptrot, M. M. Olmstead and P. P. Power, *Chem. Commun.*, 2016, **52**, 13656–13659.
73 C. Weetman, N. Ito, M. Unno, F. Hanusch and S. Inoue, *Inorganics*, 2019, **7**, 92–103.
74 H. J. Cowley, M. S. Holt, R. L. Melen, J. M. Rawson and D. S. Wright, *Chem. Commun.*, 2011, **47**, 2682–2684.
75 M. Dömling, M. Arrowsmith, U. Schmidt, L. Werner, A. C. Castro, J. O. C. Jiménez-Halla, R. Bertermann, J. Müssig, D. Prieschl and H. Braunschweig, *Angew. Chem., Int. Ed.*, 2019, **58**, 9782–9786.